REPORT DOCUMENTATION PAGE

Form Approved OMB No. 0704-0188

1. REPORT DATE *(DD-MM-YYYY)*	2. REPORT TYPE	3. DATES COVERED *(From - To)*
18/07/2007	Final Technical Report	Jan 1, 2004 - Feb 1, 2007

4. TITLE AND SUBTITLE
ROBUST MULTI-LENGTH SCALE DEFORMATION PROCESS DESIGN FOR THE CONTROL OF MICROSTRUCTURE-SENSITIVE MATERIAL PROPERTIES

5a. CONTRACT NUMBER
FA9550-04-1-0070

5b. GRANT NUMBER

5c. PROGRAM ELEMENT NUMBER

6. AUTHOR(S)
Nicholas Zabaras

5d. PROJECT NUMBER

5e. TASK NUMBER

5f. WORK UNIT NUMBER

7. PERFORMING ORGANIZATION NAME(S) AND ADDRESS(ES)

Cornell University
188 Rhodes Hall
Mechanical and Aerospace Engr
Ithaca, NY 14853-3801

8. PERFORMING ORGANIZATION REPORT NUMBER

9. SPONSORING / MONITORING AGENCY NAME(S) AND ADDRESS(ES)
Dr. Fariba Fahroo
Computat. Mathematics, AFOSR/NM
875 North Randolph Street
Arlington, VA 22203
fariba.fahroo@afosr.af.mil

10. SPONSOR/MONITOR'S ACRONYM(S)

11. SPONSOR/MONITOR'S REPORT NUMBER(S)

12. DISTRIBUTION / AVAILABILITY STATEMENT

Approved for public release. Distribution is unlimited

AFRL-SR-AR-TR-07-0358

13. SUPPLEMENTARY NOTES

14. ABSTRACT The objective of this work was to develop a robust design methodology for optimizing microstructure-sensitive properties in aircraft components manufactured using metal forming processes. The multi-scale forming design simulator developed provides means to select the sequence of deformation processes, design the dies and preforms for each process stage as well as the process conditions such that a product is obtained with desired shape and microstructure. Modeling of uncertainty propagation in such multi-scale models of deformation is extremely complex considering the nonlinear coupled phenomena that need to be accounted for. The work addresses key mathematical and computational issues related to robust multi-scale design of deformation processes. Our research accomplishments include development of new mathematical models based on spectral polynomial chaos, support space, and entropy maximization techniques for modeling sources of uncertainties in material deformation processes. These models, in conjunction with multi-scale homogenization models, allow simulations of the effect of microstructural variability on the reliability of macro-scale systems. We have developed the first stochastic variational multi-scale simulator with an explicit sub-grid model, a robust deformation process simulator using spectral and collocation methods for simulating uncertainties in metal forming processes. Finally, recent developments including an information theoretic framework for modeling microstructural uncertainties is summarized.

15. SUBJECT TERMS
Stochastic modeling; Materials; Deformation processes; Uncertainty quantification; microstructure modeling; microstructure-sensitive properties; computational design

16. SECURITY CLASSIFICATION OF: U			17. LIMITATION OF ABSTRACT	18. NUMBER OF PAGES	19a. NAME OF RESPONSIBLE PERSON
a. REPORT	b. ABSTRACT	c. THIS PAGE		25	N. Zabaras
u	u	u			19b. TELEPHONE NUMBER *(include area code)* 607 255 9104

FINAL REPORT
AFOSR CONTRACT NO. FA9550-04-1-0070

AFOSR Computational Mathematics Program 2007

ROBUST MULTI-LENGTH SCALE DEFORMATION PROCESS DESIGN FOR THE CONTROL OF MICROSTRUCTURE-SENSITIVE MATERIAL PROPERTIES

Cornell University

Principal Investigator

Dr. Nicholas Zabaras, Professor

Materials Process Design and Control Laboratory
Sibley School of Mechanical and Aerospace Engineering
188 Frank H. T. Rhodes Hall
Cornell University
Ithaca, NY 14853-3801

Email: zabaras@cornell.edu

Telephone: 607 255 9104
Fax: 607 255 1222

URL: http://mpdc.mae.cornell.edu/

Project Period: *2004 - 2007*

EXECUTIVE SUMMARY

The objective of this work is to develop a robust design methodology for optimizing microstructure-sensitive properties in aircraft components manufactured using metal forming processes. The multi-scale forming design simulator developed as a part of this project provides means to select the sequence of deformation processes, design the dies and preforms for each process stage as well as the process conditions such that a product is obtained with desired shape and microstructure. Modeling of uncertainty propagation in such multi-scale models of deformation is extremely complex considering the nonlinear coupled phenomena that need to be accounted for. The work completed in the project addresses key mathematical and computational issues related to robust multi-scale design of deformation processes. Our research accomplishments include development of new mathematical models based on spectral polynomial chaos, support space, and entropy maximization techniques for modeling sources of uncertainties in material deformation processes. These models, in conjunction with multi-scale homogenization models, allow simulations of the effect of microstructural variability on the reliability of macro-scale systems. We have developed the first stochastic variational multi-scale simulator with an explicit sub-grid model, a robust deformation process simulator using spectral and collocation methods for simulating uncertainties in metal forming processes. Finally, recent developments including an information theoretic framework for modeling microstructural [illegible] is summarized.

1 Status of effort

The most significant mathematical techniques/computational algorithms developed as a part of this project are explained briefly in this final report:

1. Development of spectral stochastic finite element method and non-intrusive stochastic Galerkin method for robust modeling and design of deformation processes [1, 2, 3]
2. Development of multi-scale sensitivity analysis for designing microstructure-sensitive properties in deformation processes [4, 5, 6].
3. Development of continuum sensitivity analysis technique for design of complex three dimensional deformation processes [7].
4. Development of stochastic variational multi-scale model with explicit subgrid modeling for solving multi-scale partial differential equations (PDEs) in random heterogeneous microstructures [8, 9].
5. Development of maximum entropy techniques for modeling topological uncertainties in polycrystalline metallic microstructures and its influence of homogenized properties.[10, 11, 12]

Detailed information on mathematical developments are available from the above papers and the thesis of students involved in the project. Preprints of the above papers and thesis copies are available for download at our web-site http://mpdc.mae.cornell.edu

2 Development of stochastic finite element techniques for robust modeling and design of deformation processes

Two approaches were developed towards modeling uncertainties in deformation processes. In the first technique, Spectral Stochastic Finite Element Method (SSFEM), a spectral expansion of the current configuration of a deforming body is proposed using Legendre chaos expansions to compute the stochastic deformation gradient which is in turn used to compute statistics of several critical quantities in large deformation analysis. A stochastic large deformation analysis following this approach is presented in our work in [1]. The second algorithm is based on a finite element representation of the support space of the random variables. This method is particularly useful for capturing instabilities and bifurcations in physical phenomena as demonstrated in [2]. The support space representation can lead to a non-intrusive decoupled as well as intrusive coupled formulation for evaluating the stochastic process. The highlight of the decoupled approach, called Non-Intrusive Stochastic Galerkin (NISG) method, is that it can be directly applied to presently available deterministic codes with minimal effort needed to compute the complete probability density function (PDF) of a stochastic process. In NISG method, the stochastic process is represented over the support space using piecewise continuous orthogonal polynomials in multi-dimensional random variables. The polynomials we choose are locally supported element shape functions used for representing functions in the finite element method. The h and p convergence characteristics of the discretized stochastic domain are identical to spatial finite elements. The SSFEM and NISG approaches are described in this section.

2.1 Spectral stochastic finite element techniques for robust modeling of deformation processes [1]

This work introduces algorithms for quantifying uncertainty propagation in finite deformation problems. The first algorithm is based on the the Spectral Stochastic Finite Element Method (SSFEM). A spectral expansion of the current configuration of a deforming body is proposed using Legendre chaos expansions to compute the stochastic deformation gradient which is in turn used to compute the stochastic analogs of the various quantities which appear in large deformation analysis. The deformation process is assumed to be quasi-static and inertial effects are ignored. A total Lagrangian FEM formulation is used to solve the

direct deformation problem in which material occupying an initial configuration $\boldsymbol{B}_0$ is deformed to obtain a configuration $\boldsymbol{B}_{n+1}$ at time $t = t_{n+1}$.

Let $\boldsymbol{X}$ be a material particle in $\boldsymbol{B}_0$ and let $\boldsymbol{x} = \boldsymbol{x}(\boldsymbol{X}, t_{n+1})$ be its location at time t_{n+1}. The total deformation gradient can be defined as

$$\boldsymbol{F}(\boldsymbol{X}, t_{n+1}) = \nabla_0 \boldsymbol{x}(\boldsymbol{X}, t_{n+1}) = \frac{\partial \boldsymbol{x}(\boldsymbol{X}, t_{n+1})}{\partial \boldsymbol{X}} \tag{2.1}$$

The total deformation gradient can then be decomposed into the elastic and plastic parts $\boldsymbol{F}^e$ and $\boldsymbol{F}^p$, respectively. In the subsequent text, we adopt the following notation. All quantities defined at the time $t = t_n$ will be denoted by the subscript n, while all the quantities without any subscript will refer to time $t = t_{n+1}$. The subscript $n+1$ will only be used explicitly wherever needed to facilitate understanding.

In the absence of body forces, the equilibrium equation at $t = t_{n+1}$ can be expressed in the initial configuration $\boldsymbol{B}_0$ as,

$$\nabla_0 \bullet \boldsymbol{P} = 0 \tag{2.2}$$

where ∇_0 denotes the divergence in $\boldsymbol{B}_0$ and $\boldsymbol{P}$ is the first Piola-Kirchhoff stress defined in the initial configuration. $\boldsymbol{P}$ is related to the Cauchy stress $\boldsymbol{T}$ defined in the current configuration as follows:

$$\boldsymbol{P} = det\boldsymbol{F}\boldsymbol{T}\boldsymbol{F}^{-T} \tag{2.3}$$

A hyperelastic constitutive law and classical J_2 flow theory for plastic deformation involving state variable based constitutive models are used. A real-valued space-time stochastic process $w(\boldsymbol{p}, t)$ with known probability distribution can be written as a function $w(\boldsymbol{p}, t, \theta)$ with $\boldsymbol{p}$, t and θ denoting dependence on space, time and the probability space, respectively. In subsequent sections, any quantity with a θ-dependence represents a random quantity and θ would be referred to as the random dimension. In the spectral stochastic approach, two different expansions, the Karhunen Loeve Expansion (KLE) and the Generalized Polynomial Chaos Expansion (GPCE) have been proposed for representing random quantities. The classical polynomial chaos expansion used in this work employs Hermite polynomials in multidimensional $\mathcal{N}(0,1)$ random variables as a trial basis for the probability space to represent a stochastic process. Let us consider a set of independent, identically distributed (iid) Gaussian random variables denoted as $\{\xi_i(\theta)\}_{i=0}^{\infty}$. The polynomial chaos representation of a random process can be written as:

$$\begin{aligned} w(\boldsymbol{x}, t, \theta) = a_0(\boldsymbol{x}, t)\Gamma_0 \quad &+ \quad \sum_{i_1=1}^{\infty} a_{i_1}(\boldsymbol{x}, t)\Gamma_1(\xi_{i_1}(\theta)) \\ &+ \quad \sum_{i_1=1}^{\infty}\sum_{i_2=1}^{i_1} a_{i_1 i_2}(\boldsymbol{x}, t)\Gamma_2(\xi_{i_1}(\theta), \xi_{i_2}(\theta)) + \ldots \end{aligned} \tag{2.4}$$

where $\Gamma_{\mathrm{p}}(\bullet)$ (popularly known as polynomial chaoses) are Hermite polynomials in $(\xi_1(\theta), \xi_2(\theta), \ldots)$. The above equation can be re-written in a compact form as follows:

$$w(\boldsymbol{x}, t, \theta) = \sum_{i=0}^{\infty} w_i(\boldsymbol{x}, t)\Phi_i(\theta) \tag{2.5}$$

where there is one-to-one correspondence between the functionals $\Gamma_{\mathrm{p}}(\bullet)$ and $\Phi_i(\theta)$. In actual practice, the random process is represented by a truncated chaos expansion with a limited number of terms. The polynomials $\{\Phi_i(\theta)\}_{i=0}^{\infty}$ form a complete orthogonal basis for the probability space. The orthogonality relationship is defined by

$$< \Phi_i \Phi_j > = < \Phi_i^2 > \delta_{ij} \tag{2.6}$$

where $< ., . >$ denotes the inner product in the Hilbert support space of the random variables ξ_i. In this work, since we only deal with uniformly distributed input and material uncertainties, Legendre polynomials are used in the PC expansion.

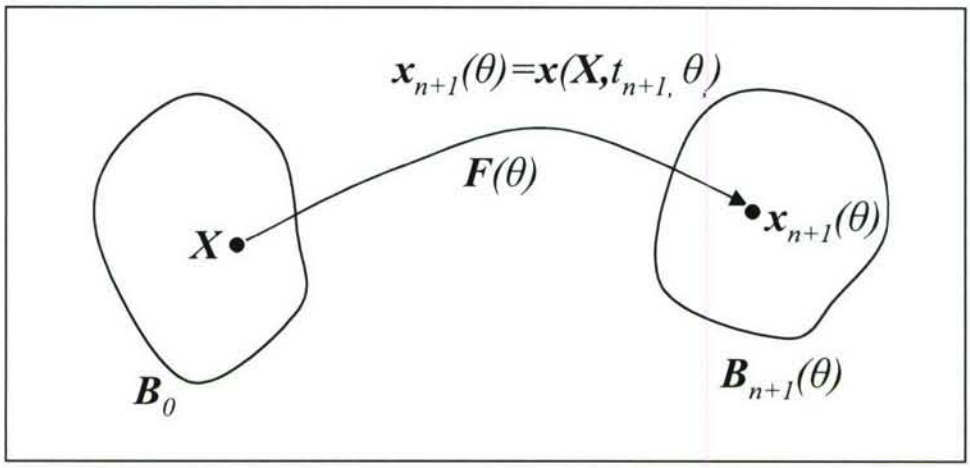

Figure 1: Stochastic motion of the deforming body.

We now proceed to develop stochastic formulations for the deterministic large deformation problem. In particular, all quantities are considered random and expanded in a polynomial chaos basis. In all the equations which will be presented, it is important to understand that the stochastic process represents an ensemble of deterministic realizations associated with a PDF. Thus the stochastic governing equations represent the governing equations for each of the deterministic realizations in the ensemble. For instance, the stochastic equilibrium equation represents an ensemble of equilibrium equations for each of the deterministic realizations comprising the stochastic process. Thus all the constraints and laws which are valid in the deterministic problem (e.g. objectivity of constitutive laws, $det\boldsymbol{F}^e > 0$, $det\boldsymbol{F}^p = 1$) are equally valid in the stochastic problem.

We start by making an assumption that the initial undeformed configuration of the body is completely deterministic. The primary variable of interest in stochastic large deformation analysis is the displacement which can be expanded as follows:

$$\boldsymbol{u}_{n+1}(\boldsymbol{x},\theta) = \sum_{i=0}^{M} \boldsymbol{u}_{n+1_i}(\boldsymbol{x})\Phi_i(\theta) \tag{2.7}$$

where, we use a truncated chaos expansion to represent the random variable.

Computing the stochastic deformation gradient The stochastic large-deformation motion of a body is considered in this section. Let the initial deterministic configuration of the body be denoted as $\boldsymbol{B}_0$. We define a stochastic motion $\boldsymbol{x}(\boldsymbol{X}, t_{n+1}, \theta)$ which deforms the body from its initial configuration to a final configuration $\boldsymbol{B}_{n+1}(\theta)$ (Fig. 1). The location of the material point $\boldsymbol{x}_{n+1}(\theta)$ in $\boldsymbol{B}_{n+1}(\theta)$ is thus defined by

$$\boldsymbol{x}_{n+1}(\theta) = \boldsymbol{x}(\boldsymbol{X}, t_{n+1}, \theta) \tag{2.8}$$

In the configuration $\boldsymbol{B}_{n+1}(\theta)$, the coordinates of the different points will be defined by the same random variables which define the motion. The stochastic position coordinates of the final configuration can be represented as $\boldsymbol{x}_{n+1} = \boldsymbol{x}_{n+1_i}\Phi_i(\theta)$. Since these position coordinates completely define the configuration of the body, we can denote $\boldsymbol{B}_{n+1}(\theta)$ as $\boldsymbol{B}_{n+1_i}\Phi_i$, where $\boldsymbol{B}_{n+1_i}$ denotes a virtual configuration defined by the points $\boldsymbol{x}_{n+1_i}$. This configuration may not have any physical interpretation but is only defined to simplify the understanding of the stochastic formulation.

Using the above definitions, the stochastic deformation gradient at time t_{n+1} can be expressed as

$$\boldsymbol{F}(\theta) = \nabla_0 \boldsymbol{x}(\boldsymbol{X}, t_{n+1}, \theta) = \frac{\partial \boldsymbol{x}(\boldsymbol{X}, t_{n+1}, \theta)}{\partial \boldsymbol{X}} \tag{2.9}$$

To ensure that the motion is well-defined, it is required that $det\boldsymbol{F}(\theta) > 0$. Thus the randomness in a meaningful motion will propagate in such a manner that the above constraint is satisfied. For a discretized

and parameterized domain such as a finite element mesh, Eq. (2.9) can be expressed as follows:

$$\boldsymbol{F}(\theta) = \boldsymbol{P}(\boldsymbol{x}_{n+1}, \theta)\boldsymbol{Q}^{-1}(\boldsymbol{X}) \tag{2.10}$$

where,

$$P_{\alpha\beta}(\boldsymbol{x}_{n+1}, \theta) = \frac{\partial x^{\alpha}_{n+1}(\theta)}{\partial \eta_{\beta}} \tag{2.11}$$

and

$$Q_{\alpha\beta}(\boldsymbol{X}) = \frac{\partial X^{\alpha}}{\partial \eta_{\beta}} \tag{2.12}$$

where η_β denotes the natural coordinates in the parameterized domain and $\alpha, \beta = 1, \ldots, nsd$ where nsd denotes the number of space dimensions of the problem. Now, we can expand $x^{\alpha}_{n+1}(\theta)$ in its polynomial chaos basis as follows

$$x^{\alpha}_{n+1}(\theta) = x^{\alpha}_{n+1_i}\Phi_i(\theta) \tag{2.13}$$

and as a result $\boldsymbol{P}$ can be written as

$$\boldsymbol{P}(\boldsymbol{x}_{n+1}, \theta) = \boldsymbol{P}_i(\boldsymbol{x}_{n+1_i})\Phi_i(\theta) \tag{2.14}$$

where each $\boldsymbol{P}_i$ denotes a $nsd \times nsd$ matrix given by

$$P_{\alpha\beta_i}(\boldsymbol{x}_{n+1_i}) = \frac{\partial x^{\alpha}_{n+1_i}}{\partial \eta_{\beta}} \tag{2.15}$$

For notational simplicity, the dependencies θ and $\boldsymbol{x}$ are dropped henceforth. Using Eqs. (2.9), (2.12) and (2.14), the deformation gradient can now be written as follows:

$$\boldsymbol{F} = \boldsymbol{F}_i\Phi_i = (\boldsymbol{P}_i\Phi_i)\,(\boldsymbol{Q})^{-1} \tag{2.16}$$

Thus, $\boldsymbol{F}_i$ can be obtained as

$$\boldsymbol{F}_i = \boldsymbol{P}_i\boldsymbol{Q}^{-1} \tag{2.17}$$

Each $\boldsymbol{F}_i$ in the above equation can be interpreted as the deformation gradient for the motion which maps the initial configuration $\boldsymbol{B}_0$ to each of the virtual configurations $\boldsymbol{B}_i$. The other quantities which appear in the principle of virtual work statement can now be derived from $\boldsymbol{F}$.

Linearized stochastic virtual work: Having computed $\boldsymbol{F}$, we now proceed to formulate the linearized virtual work equation for the stochastic finite deformation problem. The linearized stochastic virtual work can be expressed as follows:

$$\int_{\boldsymbol{B}_0} d\boldsymbol{P}.\frac{\partial \tilde{\boldsymbol{u}}}{\partial \boldsymbol{X}} dV_0 = -\int_{\boldsymbol{B}_0} \boldsymbol{P}.\frac{\partial \tilde{\boldsymbol{u}}}{\partial \boldsymbol{X}}\, dV_0 + \int_{\boldsymbol{\Gamma}} \boldsymbol{t}.\tilde{\boldsymbol{u}}\, dA_0 \tag{2.18}$$

Expanding the random variables in their polynomial chaos expansions (PCE), we obtain:

$$\int_{\boldsymbol{B}_0} d\boldsymbol{P}_i.\frac{\partial \tilde{\boldsymbol{u}}_j}{\partial \boldsymbol{X}}\Phi_i\Phi_j dV_0 = -\int_{\boldsymbol{B}_0} \boldsymbol{P}_i.\frac{\partial \tilde{\boldsymbol{u}}_j}{\partial \boldsymbol{X}}\Phi_i\Phi_j\, dV_0 + \int_{\boldsymbol{\Gamma}} \boldsymbol{t}_i.\tilde{\boldsymbol{u}}_i\Phi_i\Phi_j\, dA_0 \tag{2.19}$$

All the quantities in the above expression except $\boldsymbol{B}_0, dV_0, dA_0$ are stochastic in nature. The stochastic quantities are computed in a similar manner as in the deterministic problem using the elementary operations for random quantities described earlier. In the process of computing these quantities, analogous expressions for the stress and strain measures, consistent moduli, elastic and plastic deformation gradients as well as the stress update algorithm need to be considered.

Next we consider the term $\frac{\partial \tilde{\boldsymbol{u}}_i}{\partial \boldsymbol{X}}$ in Eq. (2.19) and noting that we use a total Lagrangian formulation, we obtain the following:

$$\frac{\partial \tilde{\boldsymbol{u}}_i}{\partial \boldsymbol{X}} = H\Delta u_i = d\boldsymbol{F}_i \tag{2.20}$$

where H is a suitably defined operator.

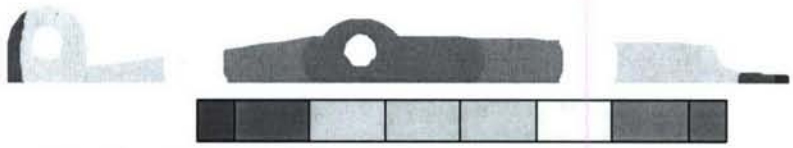

Figure 2: One of the realizations in the KL expansion of the fiber orientation (Problem 3).

On substituting Eq. (2.20) in Eq. (2.19) and discretizing the space domain using finite elements and performing the integration over the initial configuration, we arrive at an expression of the form:

$$\boldsymbol{K}_i \Phi_i \Delta \boldsymbol{u}_j \Phi_j = \boldsymbol{B}_k \Phi_k \tag{2.21}$$

Finally on considering a Galerkin projection, a linear system of equations is obtained for the unknowns $\Delta \boldsymbol{u}_j$ given by

$$\boldsymbol{K}_i \Delta \boldsymbol{u}_j < \Phi_i \Phi_j \Phi_l >= \boldsymbol{B}_l < \Phi_l^2 > \tag{2.22}$$

Thus using the definition of $\boldsymbol{F}$ and the various operations on random matrices and scalars a complete stochastic formulation of the hyperelastic-viscoplastic finite deformation problem can be obtained.

Numerical Example: Effect of uncertain fiber orientation on the response of a composite material

In this problem, we examine the effect of uncertain fiber orientation on the response of a typical aerospace component made of a composite material. The 2D section of a nozzle flap is shown in Figure 2. Plane strain conditions are assumed. The total length is taken as 1 mm. Other dimensions are assumed accordingly. The flap is subjected to an aerodynamic force (uniform pressure) on its back. The pin-eyes are assumed rigidly fixed. The material is assumed to be orthotropic-hyperelastic. An orthotropic Neo-Hookean strain energy function is considered for the problem which leads to a non-constant Lagrangian elasticity tensor given by

$$\begin{aligned} \boldsymbol{\mathcal{L}}^e &= \lambda det\boldsymbol{F}(2det\boldsymbol{F}-1)\bar{\boldsymbol{C}}^{-1} \otimes \bar{\boldsymbol{C}}^{-1} + 2[\mu + \lambda det\boldsymbol{F}(det\boldsymbol{F}-1)]\boldsymbol{G} \\ &+ 8\gamma \boldsymbol{a} \otimes \boldsymbol{a} \otimes \boldsymbol{a} \otimes \boldsymbol{a} + 4\beta(\boldsymbol{a} \otimes \boldsymbol{a} \otimes \boldsymbol{I} + \boldsymbol{I} \otimes \boldsymbol{a} \otimes \boldsymbol{a}) - \alpha \boldsymbol{A} \end{aligned} \tag{2.23}$$

The vector $\boldsymbol{a}$ denotes the unit fiber axis. For the 2D case, it can be written as $(cos\theta, sin\theta, 0)$. For the stochastic problem, we consider the fiber orientation to be uncertain with the initial fiber angle defined by a KL expansion using a covariance kernel. An exponential covariance kernel was assumed which is given by

$$\mathcal{R}(\boldsymbol{p}_1, 0, \boldsymbol{p}_2, 0) = (\sigma)^2 exp(\frac{-r}{b}) \tag{2.24}$$

where r is the distance between the points $\boldsymbol{p}_1$ and $\boldsymbol{p}_2$. b is the correlation length and is assumed to be 1 mm and $\sigma = 0.3$. Thus, the fiber orientation can be written as,

$$\theta(\boldsymbol{p}) = \sum_{i=1}^{\infty} \xi_i \sqrt{\lambda_n} f_i(\boldsymbol{p}) \tag{2.25}$$

where the mean fiber orientation is assumed to be along the x-axis. We assume that the flap is composed of short fibers which justifies the above model for considering heterogeneity in the fiber orientation. For this problem, we consider terms up to $i = 2$ in the KL expansion. A comparatively large uniform pressure of 0.002 N/mm^2 is applied at the back of the flap. An order 3 PCE is used leading to 10 terms in the expansion. Figure 2 shows one of the realizations of the heterogeneity in the fiber orientation. The stochastic mean solution shows a considerable deviation from the deterministic solution. The mean and standard deviation of the equivalent stress are plotted in Fig. 3.

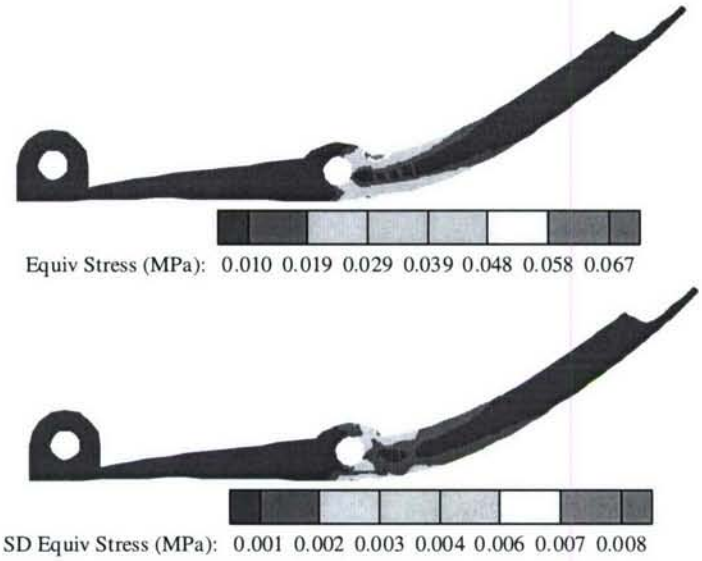

Figure 3: Mean (top) and standard deviation (bottom) of the equivalent stress using order 3 PCE (Problem 3).

2.2 Non-intrusive stochastic Galerkin scheme for robust modeling of deformation processes [2]

In this method, the stochastic process is represented over the support space using piecewise continuous orthogonal polynomials in multi-dimensional random variables. The polynomials we choose are the locally supported element shape functions of a specific order used for representing functions in the finite element method. The space Θ spanned by these random variables is discretized using disjoint finite element subdomains leading to a new discretized space Θ^h where h is an element size parameter. This approximation can be denoted as

$g(\boldsymbol{x}, t, \theta) = g(\boldsymbol{x}, t, \xi_1, \xi_2, ..) \approx g^h(\boldsymbol{x}, t, \xi_1, \xi_2, ..\xi_N) = g^h(\boldsymbol{x}, t, \boldsymbol{\xi})$.

Thus the stochastic process can be represented using the basis functions as

$$g^h(\boldsymbol{x}, t, \boldsymbol{\xi}) = \sum_{i=1}^{nodes} g_i^h \Phi_i(\boldsymbol{\xi}) \tag{2.26}$$

where Φ_i are the locally supported basis functions and g_i are the corresponding nodal values. A scheme for discretization of a one dimensional ($N = 1$) pdf is shown in Fig.4

It was shown in [13] that for functions involving high nonlinearities and critical points the GPCE fails to perform satisfactorily. On the other hand, a piecewise representation is ideally suited for representing discontinuities and nonlinearities in the processes. As mentioned before, finite deformation processes involve considerable degrees on nonlinearities at every stage. Thus we resort to the third approach - a piecewise representation using finite element basis functions for representation of the random large deformation processes in this work. This is also advantageous from a practical point of view since in converting a deterministic finite element based deterministic large deformation code to simulate stochastic deformation processes, these basis functions are available from other parts of the code and can be readily used for representing random functions.

The piecewise representation of the stochastic process which was discussed in the previous section, can lead to a non-intrusive decoupled as well as intrusive coupled formulation for evaluating the stochastic process. The two formulations are explained with an example of a solution of a linear system. We consider the evaluation of a random vector $u(\boldsymbol{x}, \boldsymbol{\xi})$ by the solution of a linear system which is defined by a random matrix $A(\boldsymbol{\xi})$ and a random vector $b(\boldsymbol{\xi})$ as shown below. (The superscript h has been dropped for notational

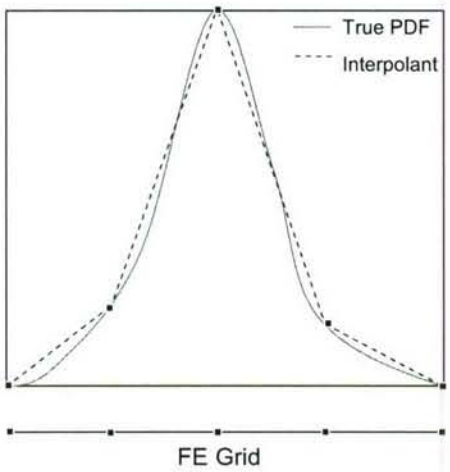

Figure 4: Finite Element discretization scheme for a 1 dimensional pdf

simplicity)

$$A(\boldsymbol{x},\boldsymbol{\xi})u(\boldsymbol{x},\boldsymbol{\xi}) = b(\boldsymbol{x},\boldsymbol{\xi}) \tag{2.27}$$

Intrusive Coupled system To solve the system using the coupled formulation, we first represent the above process in a N dimensional piecewise polynomial basis (equivalent to N nodes in the mesh)

$$A_i(\boldsymbol{x})\Phi_i(\boldsymbol{\xi})u_j(\boldsymbol{x})\Phi_j(\boldsymbol{\xi}) = b_k(\boldsymbol{x})\Phi_k(\boldsymbol{\xi}) \tag{2.28}$$

where $i, j, k = 1 \ldots N$. Thus the solution of the random vector u involves computing the coefficients u_j in the polynomial representation from the known values of A_i and b_k. This is done by projecting (inner product) the above equation into each orthogonal basis function Φ_l leading to

$$A_i u_j < \Phi_i\Phi_j\Phi_l >= b_k < \Phi_k\Phi_l > \tag{2.29}$$

where the inner product is defined as follows

$$< x(\boldsymbol{\xi})y(\boldsymbol{\xi}) >= \int_\Theta xyf(\boldsymbol{\xi})d\boldsymbol{\xi} \tag{2.30}$$

Using the orthogonality relation of the polynomials basis functions in Eq. 2.29 we get

$$A_i u_j < \Phi_i\Phi_j\Phi_l >= b_k < \Phi_l^2 > \delta_{lk} = b_l < \Phi_l^2 > \tag{2.31}$$

Thus evaluation of the u_j's involves solution of a coupled system. The coupled system involves $N \times ndof$ equations. Moreover, it needs explicit representations of the stochastic processes $a(\boldsymbol{\xi})$ and $b(\boldsymbol{\xi})$ in terms of the basis functions which may not be readily available and may involve more intrusive computations and change of the overall structure of the underlying deterministic code.

Decoupled system - NISG formulation

In the non-intrusive decoupled scheme, the output stochastic process is constructed using deterministic function evaluations at an optimal number of points defined in the input support space. Considering the linear system (Eq. 2.27) again at specific points $\boldsymbol{\xi}_i$ of the support space we get

$$A(\boldsymbol{x},\boldsymbol{\xi}_i)u(\boldsymbol{x},\boldsymbol{\xi}_i) = b(\boldsymbol{x},\boldsymbol{\xi}_i) \tag{2.32}$$

As can be observed, each function evaluation of A, u and b takes place at fixed points $\boldsymbol{\xi}_i$ in the random space. This can be equivalently expressed as

$$A_i(\boldsymbol{x})u_i(\boldsymbol{x}) = b_i(\boldsymbol{x}) \tag{2.33}$$

The above system can be solved for u_i at predetermined points of the support space which can be used to construct the solution u($\boldsymbol{x}$,$\boldsymbol{\xi}$). The procedure is explained later in the section.

The specific function evaluation points are chosen from the consideration that in typical problems involving random variables, the quantities of interest are the probability density function, and the statistical moments of u. The p^{th} statistical moment can be calculated as follows:

$$M_p = \int_{\Theta} (u(\boldsymbol{x}, t, \boldsymbol{\xi}))^p f(\boldsymbol{\xi}) d\boldsymbol{\xi} = \sum_{e=1}^{nel} \int_{\Theta^e} (u(\boldsymbol{x}, t, \boldsymbol{\xi}))^p f(\boldsymbol{\xi}) d\boldsymbol{\xi} \tag{2.34}$$

where nel is the number of elements in the support space while Θ^e represents the local element domain. Using a Gauss quadrature integration scheme with n integration points per element, the above expression can be approximated as:

$$M_p \approx \tilde{M}_p = \sum_{e=1}^{nel} \sum_{i=1}^{n} w_i (u(\boldsymbol{x}, t, \boldsymbol{\xi}_i))^p f(\boldsymbol{\xi}_i) \tag{2.35}$$

where $\boldsymbol{\xi}_i$ denote the abscissae of the integration points while w_i denote the respective weights.

The above equation can be equivalently expressed as:

$$\tilde{M}_p = \sum_{e=1}^{nel} \sum_{i=1}^{n} w_i (u_i(\boldsymbol{x}, t))^p f(\boldsymbol{\xi}_i) \tag{2.36}$$

where $u_i(\boldsymbol{x}, t)$ denotes a deterministic space-time dependent process at each integration point of the support space.

Thus evaluation of u_i is completely deterministic and can be achieved using a readily available deterministic solution scheme and hence the non-intrusive terminology. To obtain the pdf of u denoted as $f_u(\boldsymbol{\xi})$, we first obtain the values of u at the nodal points of the discretized random space from the integration point values u_i. This can be achieved using a standard least squares smoothing scheme. $f_u(\boldsymbol{\xi})$ can then be obtained by generating random Monte Carlo samples from the pdfs of the input random variables $\boldsymbol{\xi}$, followed by evaluations of u at those points. It should be noted that this sampling does not require an explicit function evaluation but is generated from an interpolation of earlier evaluations using the appropriate interpolation order.

The developed scheme for discretization of the stochastic support space closely follows the finite element discretization of spatial domains in various applications and inherits all its properties. The the h and p convergence characteristics of the discretized domain are identical to the case of spatial finite elements.

The procedure for NISG analysis of large deformation processes can be summarized as follows.

1. Determine the pdf of the input uncertainties in terms of independent random variables $\{\xi_i\}_{i=1}^{N}$ and compute the joint pdf $f(\boldsymbol{\xi})$.

2. Determine the dimensionality of the support space. Based on this dimension discretize the support space using finite elements.

3. FOR j=1 to number of elements in the grid

   FOR i=1 to number of local element integration points

   Compute the values of the random inputs at the support space integration point

   Solve the deterministic large deformation problem with the given inputs and compute u_i - the output of interest.

   END

   END

4. Compute u from the values of u_i using least squares smoothing.

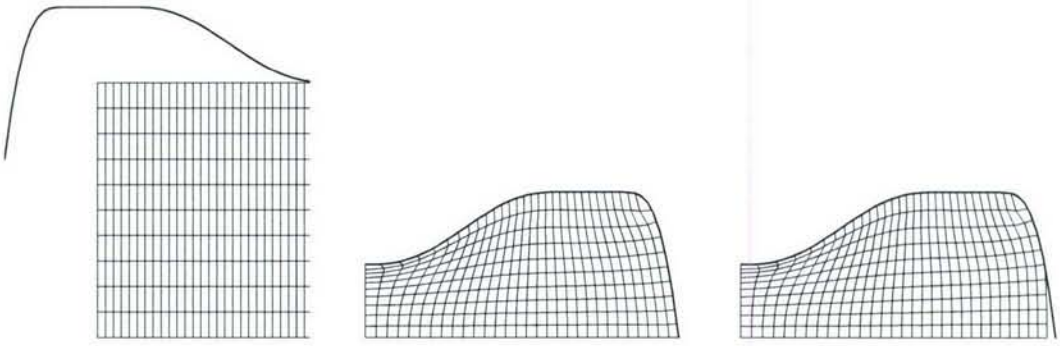

Figure 5: Initial configuration (left), final configuration with no initial voids (center) final configuration with an initial void fraction of 0.03.

5. Compute the moments as required from the u_i values as described in Eq. 2.35

Thus, the NISG approach involves deterministic function evaluations at the integration points of the discretized support space of random variables which essentially translates to a decoupled approach for evaluating the additional degrees of freedom resulting from the randomness in the problem. The computational gains attained by this decoupling are significant. Also these gains can offset to a great extent the issue of slower convergence rate compared to GPCE by the selection of a finer grid for the support space.

NISG Example - Stochastic estimation of die underfill caused by material porosity

This problem studies the effect of a random voids in the design of flashless closed die forging processes. The material is chosen to be an Fe-2% Si alloy at 1273 K. A hyperbolic sine flow function is assumed. The die-workpiece friction coefficient was taken as 0.1. For an initial billet (dimensions - radius .9339mm, height 1 mm) with no voids having the same volume as the die ($2.74mm^3$), the deterministic flashless closed die forging process is shown in Fig. 5. The corresponding final state for the deterministic process with an initial void fraction of 0.03 in the billet is also shown in the same figure. In the regions where there are compressive stresses, the void fraction decreases leading to a decrease in volume. The converse happens in regions of tensile stresses. As a result an underfill is observed in the process.

The NISG technique provides a robust way to estimate the statistics of the extent of die underfill as a result of a random distribution of voids in the billet. The initial void distribution is derived from an assumed exponential correlation kernel using a Karhunen Loéve expansion given by :

$$\mathcal{R}(\boldsymbol{p}_1, 0, \boldsymbol{p}_2, 0) = \sigma^2 exp(\frac{-r}{b}) \tag{2.37}$$

where r is the distance between the points $\boldsymbol{p}_1$ and $\boldsymbol{p}_2$, b is the correlation length assumed to be 5 mm and $\sigma = 0.1$. As in the earlier example, a truncated KL expansion sufficient to represent the heterogeneities for the stochastic void fraction can be written as,

$$f(\boldsymbol{p}) = f_0(1 + \sum_{i=1}^{2} \xi_i \sqrt{\lambda_n} f_i(\boldsymbol{p})) \tag{2.38}$$

where $f_0 = 0.03$ is the mean void fraction. A 9x9 grid was used for computing the statistics. The mean underfill was estimated to be $0.046976mm^3$ with a standard deviation of $0.0022mm^3$. Using a 10x10 support space grid the mean underfill was found to be $0.046187mm^3$ with a standard deviation of $0.0023mm^3$. The complete pdf of the underfill observed is plotted in Fig.6

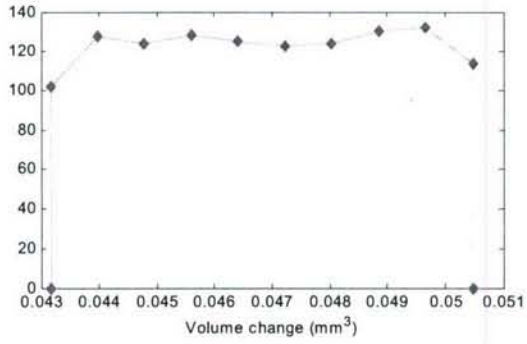

Figure 6: Probability distribution of the underfill observed due to material porosity in the flashless closed die forging problem.

3 Development of multi-scale sensitivity analysis for designing microstructure-sensitive properties in deformation processes

We have developed a versatile multi-scale design simulator for tailoring properties of materials by altering die and preform shapes in industrial forming processes. The problem is a significant computational challenge since a multi-scale design problem for modeling 3D processes approaches a billion degrees of freedom. We have recently acquired a 128 Intel processor Linux supercomputing cluster with funding from Department of Defense (DURIP-05) for solving such problems in materials-by-design. The mathematical developments are briefly explained in this section.

Consider a macroscopic material point and let it be associated with the underlying microstructure $\mathcal{M}$. Assume that the response of any crystal of the polycrystal is determined by its orientation $\boldsymbol{R}$, which is the rotation relating the crystal lattice frame, $\hat{\boldsymbol{e}}_i$, to a sample reference frame $\boldsymbol{e}_i$ as $\boldsymbol{e}_i = \boldsymbol{R}\,\hat{\boldsymbol{e}}_i$. The ODF (orientation distribution function), represented as $\mathcal{A}(\boldsymbol{r})$, describes the crystal density over the fundamental region. A re-orientation map, $\hat{\boldsymbol{r}}$, is associated with the ODF as, $\mathcal{A}(\boldsymbol{r},t) = \mathcal{A}(\hat{\boldsymbol{r}}(\boldsymbol{s},t),t) = \hat{\mathcal{A}}(\boldsymbol{s},t)$. The representation of the ODF given by $\mathcal{A}(\boldsymbol{r},t)$ is Eulerian and $\hat{\mathcal{A}}(\boldsymbol{s},t)$ is Lagrangian.

The evolution of a polycrystal generally demands the numerical solution of an ODF conservation equation. The conservation equation for the ODF in the Lagrangian description can be written as:

$$\int \left(\hat{\mathcal{A}}(\boldsymbol{s},t)\; J(\boldsymbol{s},t) \;-\; \hat{\mathcal{A}}(\boldsymbol{s},0)\right)\; dv \;=\; 0 \tag{3.1}$$

where dv is the volume element on the reference fundamental region, $J(\boldsymbol{s},t) = \det(\nabla\hat{\boldsymbol{r}}(\boldsymbol{s},t))$ is the Jacobian determinant of the re-orientation of the crystals and $\hat{\mathcal{A}}(\boldsymbol{s},0) = \mathcal{A}_0(\boldsymbol{s})$ is the ODF associated with the reference map and can be thought of as the initial texturing of the material. The ODF is the microstructural feature associated with every material point in a simulation of industrial forming process. The two-length scale sensitivity framework for designing deformation processes to control properties is shown in Fig. 7.

The mathematical definition of the optimization problem for the control of microstructure-sensitive properties is stated as follows:

$$\min_{\boldsymbol{\beta}} \mathcal{F}(\boldsymbol{\beta}) \quad = \int_{\mathcal{R}} (\Omega(x,r;\boldsymbol{\beta}) - \Omega^{desired}(x))^2\; dV \tag{3.2}$$

where $\Omega^{desired}$ is the desired material property represented at a material point on the final product and $\boldsymbol{\beta}$ is the design parameter to be selected. The optimization problem involves the gradient of the property Ω with respect to the process parameters, represented as: $\nabla\Omega = \left(\frac{\partial\Omega}{\partial\beta_1}, \frac{\partial\Omega}{\partial\beta_2}, \ldots, \frac{\partial\Omega}{\partial\beta_n}\right)$. The needed gradient information for optimization analysis will be computed as:

$$\frac{\partial\Omega}{\partial\beta_i} \;=\; \frac{\overset{\circ}{\Omega}\,(r,t,\beta_1,\beta_2,\ldots,\beta_n,0,\ldots,0,\Delta\beta_i,0,\ldots,0)}{\Delta\beta_i} \tag{3.3}$$

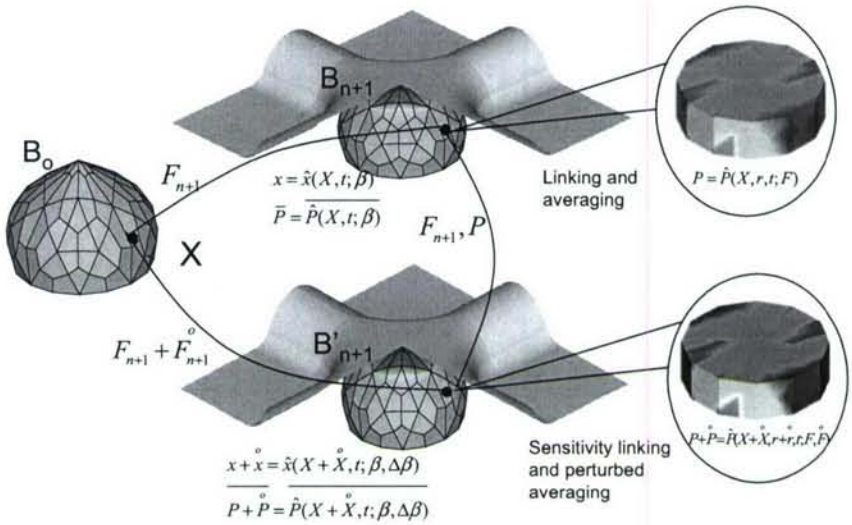

Figure 7: *Description of the parameter sensitivity analysis involved in a two-scale deformation problem. The macro-process design variable(s) control the deformation gradient at each material point. These macro-fields define the underlying microstructure and properties at the material point. In the micro-sensitivity analysis, we compute how small perturbations in the deformation gradient at the material point affects microstructure evolution. On the macro-sensitivity analysis, this perturbation to the deformation gradient at each material point is induced by the perturbations to the macro-design variables. Knowing how a macro design variable affects microstructure-sensitive properties will allow us to provide feasible materials design obtainable through processing.*

where $\overset{\circ}{\Omega}$ represents the sensitivity of Ω (with respect to the design parameters $\boldsymbol{\beta}$). Since each property of the polycrystal is obtained by averaging relations, it is essential in the proposed analysis to compute the sensitivity of texture evolution with respect to the process design parameters $\boldsymbol{\beta}$.

Computation of sensitivity of microstructure would involve computation of sensitivity of evolution of volume fractions of different crystal orientation components over the deformation history. This is computed by differentiating the ODF evolution equation in order to account for sensitivity of ODF to process variables. Consider the Lagrangian version of the ODF conservation equation (Eq. (3.1)). Design differentiation of this equation, assuming that the initial texture is independent of the design parameters ($\boldsymbol{\beta}$), leads to the following:

$$\int_{\Omega} (\overset{\circ}{\hat{\mathcal{A}}}\,(\boldsymbol{s},t;\boldsymbol{\beta},\Delta\boldsymbol{\beta})\; J(\boldsymbol{s},t;\boldsymbol{\beta}))d\Omega = -\int_{\Omega} \hat{\mathcal{A}}(\boldsymbol{s},t;\boldsymbol{\beta})\;\; \overset{\circ}{J}\,(\boldsymbol{s},t;\boldsymbol{\beta},\Delta\boldsymbol{\beta})d\Omega \tag{3.4}$$

where $\overset{\circ}{J}\;(\boldsymbol{s},t;\boldsymbol{\beta},\Delta\boldsymbol{\beta}) \;=\; \overset{\circ}{\det(\nabla\hat{\boldsymbol{r}}(\boldsymbol{s},t;\boldsymbol{\beta},\Delta\boldsymbol{\beta}))} \;=\; J(\boldsymbol{s},t;\boldsymbol{\beta})\left[\nabla_{\bullet}\;\overset{\circ}{\boldsymbol{r}}\;(\boldsymbol{s},t;\boldsymbol{\beta},\Delta\boldsymbol{\beta})\right]$. Here, sensitivities of the reorientation vector ($\overset{\circ}{\boldsymbol{r}}$) is calculated using sensitivity of the elastic part of deformation gradient computed by differentiating parameters in the constitutive integration algorithm with respect to process parameters of interest.

Once the sensitivity field for the ODF is obtained, it is straightforward to compute the sensitivities of Cauchy stress for use in the macro- sensitivity equations using sensitivity-averaging laws. Evolution of properties such as yield strength and Youngs modulus can be tracked and controlled at each point in the forged component by knowing the sensitivities of these parameters to the process variables.

Described below is the analysis for the development of a total Lagrangian sensitivity formulation for the kinematic problem at the macro-scale. Let the reference configuration be $\mathcal{B}_0$. The design differentiation of

the macro-scale equilibrium equation results in:

$$\overset{\circ}{\overline{\nabla_0 \cdot \langle \boldsymbol{P} \rangle}} + \overset{\circ}{\boldsymbol{f}} = \boldsymbol{0} \tag{3.5}$$

where $\langle \boldsymbol{P} \rangle$ is the polycrystal averaged PK-I stress. A variational form for the sensitivity equilibrium equation (for parameter sensitivity) can be posed as follows: Evaluate $\overset{\circ}{\boldsymbol{x}} = \overset{\hat{\circ}}{\boldsymbol{x}}(\boldsymbol{X}, t; \boldsymbol{\beta}, \Delta\boldsymbol{\beta})$ such that

$$\int_{\mathcal{B}_0} \overset{\circ}{\langle \boldsymbol{P} \rangle} \cdot \nabla_0 \tilde{\boldsymbol{\eta}} dV_0 = \int_{\partial \mathcal{B}_0} \overset{\circ}{\boldsymbol{\lambda}} \cdot \tilde{\boldsymbol{\eta}} \, dA_0 \tag{3.6}$$

for every $\tilde{\boldsymbol{\eta}}$, a kinematically admissible sensitivity deformation field expressed over the reference configuration $\mathcal{B}_0$. Details on the methodologies to obtain sensitivities for three-dimensional die and preform design problems, and to model sensitivities of die-workpiece contact through design-differentiation of a regularized contact problem can be found in our work in [7]. Once the final sensitivities of the texture to process variables is found at the end of simulation of a deformation process, a variety of gradient optimization algorithms can be invoked to minimize the objective function defined in Eq. (3.2) for tailoring the property distribution in the material.

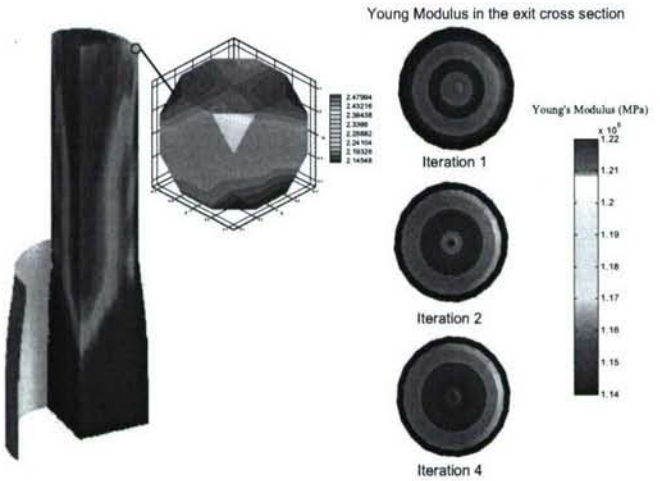

Figure 8: *Control of Youngs Modulus variation in the exit cross-section by designing optimal die shapes. (a) shows Youngs Modulus distribution at the end of the extrusion process on a sample. The polycrystalline texture at a point in the exit cross section is indicated. (b) Variation in the Youngs Modulus at the exit cross section for different die designs. Optimal design is achieved in the fourth iteration.*

Here, we show optimization of Youngs Modulus variation in the exit cross-section during metal extrusion. Fig. 8 shows Youngs Modulus distribution at the end of the extrusion process on a sample. The polycrystalline texture at all points in the exit cross section is controlled by modification of die shapes. The efficiency of the methodology is exemplified by achievement of optimal Youngs Modulus distribution in only four iterations. The variation in the Youngs Modulus at the exit cross section for different die designs are compared in Fig. 8(b). In this problem the objective was designed so as to minimize the variation of Youngs Modulus over the exit cross section.

4 Development of continuum sensitivity analysis technique for design of complex three dimensional deformation processes.

We have extended the sensitivity analysis technique to allow design of complex 3D deformation processes. In extending the design simulator to realistic 3D simulations some important issues were addressed. For complex dies, as is usually encountered in realistic metal forming simulations, die surfaces were generated using finite element meshes followed by the construction of a smooth surface from the individual element patches. We employ Gregory patches for construction of a smooth surface by interpolating the finite element nodes. This also provides tangential and normal continuity between adjacent patches. In this work automatic hexahedral

Figure 9: Initial preform and final forged product for the steering link problem (Example 6).

remeshing was implemented using the meshing software CUBIT. The specific remeshing algorithm that was used is known as THEX. In this approach an unstructured hexahedral mesh is generated by first meshing the workpiece with a tetrahedral mesh following by division of each tetrahedron into four hexes. To aid in speeding up the solution process for complex forging processes, the design simulator was parallelized using MPI. The simulator was dynamically linked to the parallel toolbox PetSc for parallel assembly and solution of linear systems. In particular, for solution of linear systems a GMRES solver along with block Jacobi and ILU preconditioning from the PetSc toolbox was employed.

Numerical Example: Isothermal preform design for a steering link

The example deals with the isothermal preform design for a steering link to ensure the required shape is obtained while the material wastage is minimized. The flow rule for the alloy is given by

$$f = \dot{\epsilon_0} \left(\frac{\bar{\sigma}}{s} \right)^n \tag{4.1}$$

where $\dot{\epsilon_0} = 0.002\ s^{-1}$, $s = 150$ MPa and $n = 5$ while the elastic parameters are taken as $\lambda = 14423$ MPa and $\mu = 9615.4$ MPa.

For the optimization problem we start with an initial preform shape which is a cylinder of much smaller volume than the volume of the die cavity (Fig.9). The preform surface is discretized using two design variables which are essentially the radii at the two ends of the cylinder while the length of the cylinder is fixed. The forging velocity was assumed to be 0.01mm/s while the stroke was fixed at 0.38 mm. The total simulation time was 38 seconds and partially adaptive remeshing operations were performed every 3 seconds. The number of elements varies between 26000 and 40000 during the remeshing operations within the optimization iterations. Using symmetry only one-eighth of the actual domain evolution is simulated. The BFGS algorithm was used for the gradient optimization process. The preform shape and the final forged product for the optimal iteration are shown in Fig. 10.

5 Development of stochastic variational multi-scale model with explicit subgrid modeling

The focus of this work is to model uncertainty induced by micro-scale variability on the macro-scale outcomes. We have developed mathematical models for direct incorporation of the inherent randomness and the effect of modeling assumptions in the design of upscaling methods. The potential applications for the problem include solving PDEs in random heterogeneous microstructures, which is a key problem of interest. Heterogeneous microstructure realizations exhibit property variations at a much smaller scale compared to the size of the computational domain D. Performing a fully-resolved calculation on these microstructures becomes computationally expensive. We consider a computational scheme that involves solving for a coarse-solution while capturing the effects of the fine scale on the coarse solution.

Figure 10: Optimal preform and final forged product for the steering link problem (Example 6).

Problem definition and variational formulation Let $\mathcal{D}$, $\mathcal{T}$ and Ω denote a closed polygonal domain, a time interval and a suitable probability space, respectively. The transient diffusion in a heterogenous medium with a spatially varying random diffusion coefficient $k(\mathbf{x},\omega)$ can be written as the following stochastic partial differential equation (SPDE):

$$u_{,t} = \nabla \cdot (k(\mathbf{x},\omega)\nabla u) + f(\mathbf{x},t,\omega),\ \mathbf{x} \in \mathcal{D},\ t \in \mathcal{T} \text{ and } \omega \in \Omega, \tag{5.1}$$

where, $u_{,t}$ denotes the partial time derivative $\partial u/\partial t$. The solution $u \equiv u(\mathbf{x},t,\omega)$ and the source term $f(\mathbf{x},t,\omega)$ are real-valued space-time stochastic fields. For closure, we also assume the following initial and boundary conditions:

$$u(\mathbf{x},t,\omega) = u_g(\mathbf{x},t,\omega),\ \mathbf{x} \in \partial\mathcal{D},\ t \in \mathcal{T} \text{ and } \omega \in \Omega, \tag{5.2}$$

$$u(\mathbf{x},0,\omega) = u_0(\mathbf{x},\omega),\ \mathbf{x} \in \mathcal{D}, \text{ and } \omega \in \Omega. \tag{5.3}$$

The variational formulation for Eqs. (5.1)–(5.3) can now be written as: Find $u \in U$ such that for all $v \in V$

$$(u_{,t}\,, v) + (k\nabla u, \nabla v) = (f, v), \tag{5.4}$$

where

$$(u, v) \stackrel{\text{def}}{=} \int_\Omega \int_{\mathcal{D}} uv \mathrm{d}\mathbf{x}\mathrm{d}\mathcal{P}. \tag{5.5}$$

Additive scale decomposition and variational multiscale method In the variational multiscale approach, we consider the exact solution u to be made up of contributions from two different scales, namely, the coarse-scale solution u^C, that can be resolved using a coarse-mesh and a subgrid solution u^F. In short, $u = u^C + u^F$. The main idea behind the VMS (operator upscaling) method is to develop models for characterizing the effect of the subgrid solution on the coarse-scale solution and to subsequently derive a modified coarse-scale formulation that only involves u^C. In order to do that, we split the variational formulation given in Eq. (5.4) as the following coarse-scale and subgrid equations: Find $u^C \in U^C$ and $u^F \in U^F$ such that

$$(u^C{}_{,t} + u^F{}_{,t}\,, v^C) + (k\nabla u^C + k\nabla u^F, \nabla v^C) = (f, v^C),\ \forall\ v^C \in V^C, \tag{5.6}$$

$$(u^C{}_{,t} + u^F{}_{,t}\,, v^F) + (k\nabla u^C + k\nabla u^F, \nabla v^F) = (f, v^F),\ \forall\ v^F \in V^F. \tag{5.7}$$

We will now proceed to solve Eq. (5.7) by applying localization assumptions to obtain an approximate model for the subgrid solution u^F. Subsequently, we will use the model for subgrid solution to eliminate u^F in Eq. (5.6) to obtain a modified formulation defined only in terms of u^C. **Subgrid modeling** Assume that the spatial domain is discretized using a coarse-mesh into disjoint sub-domains $\mathcal{D}^{(e)}, e = 1, \ldots, \text{Nel}$, where, (e) denotes the sub-domain number. We will refer to these sub-domains as "coarse elements". Let each coarse element be further discretized using a subgrid mesh into "$\text{Nel}^F_{(e)}$" disjoint sub-domains (also referred to as "subgrid elements").

We will now assume that the subgrid solution is a sum of two components $\hat{u}^F$ and u^{F0} that obey the following variational equations:

$$(u^C{}_{,t}, v^F) + (\hat{u}^F{}_{,t}, v^F) + (k\nabla u^C, \nabla v^F) + (k\nabla \hat{u}^F, \nabla v^F) = 0, \tag{5.8}$$

$$(u^{F0}{}_{,t}, v^F) + (k\nabla u^{F0}, \nabla v^F) = (f, v^F), \tag{5.9}$$

where, $\hat{u}^F$ incorporates entire coarse-scale solution information and u^{F0} is independent of the coarse-scale solution. The dynamics of u^{F0} is driven by the projection of the source term $f(\mathbf{x}, t, \omega)$ onto the subgrid trial function space V^F.

By Eq. (5.8), the term $\hat{u}^F$ behaves as a mapping from coarse-scale solution to the subgrid solution. Hence, we refer to $\hat{u}^F$ as the coarse-to-subgrid (C2S) map. Owing to the affine nature of Eq. (5.9), we shall refer to u^{F0} as the affine correction term. In order to localize the calculations of the subgrid solution, we will consider restrictions of Eqs. (5.8) and (5.9) to each coarse element $\mathcal{D}^{(e)}$. The derivations in subsequent discussion are performed for a single coarse element $\mathcal{D}^{(e)}$.

C2S map and multiscale basis functions Let us assume that in a fully-resolved direct numerical simulation, the dynamics of the exact solution can be captured using a fine time-step of δt. Since the length scales of interest in the coarse solution are far greater than the smallest length scale in the exact solution, we assume that the coarse time-step Δt is much larger in comparison to δt. Let us consider a coarse time-step $\Delta t = [t_{\mathrm{n}}, t_{\mathrm{n+1}}]$. Let t' be the local time coordinate defined such that at t_{n}, $t' = 0$ and at $t_{\mathrm{n+1}}$, $t' = \Delta t$.

Let us also assume a piecewise polynomial finite element representation for the coarse solution inside a coarse element $\mathcal{D}^{(e)}$ (please note that (e) is suppressed henceforth to simplify notation):

$$u^C(\mathbf{x}, t, \omega) = \sum_{\beta=1}^{\mathrm{Nbf}} u^C_\beta(t', \omega)\Psi_\beta(\mathbf{x}), \tag{5.10}$$

where, Nbf denotes the number of finite-element shape functions (piecewise polynomials) defined on the coarse element [8, 9]. Let us further assume a truncated generalized polynomial chaos expansion with $P_C + 1$ terms for each of the coefficients $u^C_\beta(t', \omega)$

$$u^C_\beta(t', \omega) = \sum_{s=0}^{\mathrm{P_C}} u^C_{\beta s}(t')\zeta_s(\omega). \tag{5.11}$$

Thus, the stochastic finite-element (spatial finite-element + GPCE) representation of the coarse solution can be written using local time coordinate as

$$u^C(\mathbf{x}, t, \omega) = \sum_{\beta=1}^{\mathrm{Nbf}} \sum_{s=0}^{\mathrm{P_C}} u^C_{\beta s}(t')\zeta_s(\omega)\Psi_\beta(\mathbf{x}), \tag{5.12}$$

where, $u^C_{\beta s}(t')$ denotes the nodal solution (each node has $P_C + 1$ degrees of freedom) and $\zeta_s(\omega)$ are polynomials from the hypergeometric Askey series. The form of Eq. (5.12) has been used in our earlier works [8, 9].

For the C2S map $\hat{u}^F$, we seek a representation similar to Eq. (5.12):

$$\hat{u}^F(\mathbf{x}, t, \omega) = \sum_{\beta=1}^{\mathrm{Nbf}} \sum_{s=0}^{\mathrm{P_C}} u^C_{\beta s}(t')\phi^F_{\beta s}(\mathbf{x}, t', \omega). \tag{5.13}$$

The fine-scale variational formulation of Eq. (5.8) can be re-written after substitution of Eqs. (5.12) and (5.13) is simplified as follows:

$$\left(\left\{u^C_{\beta s}(\zeta_s\Psi_\beta + \phi^F_{\beta s})\right\}_{,t}, v^F\right) + \left(k\nabla\left\{u^C_{\beta s}(\zeta_s\Psi_\beta + \phi^F_{\beta s})\right\}, \nabla v^F\right) = 0. \tag{5.14}$$

Without loss of generality, we can assume the following representation for the coarse-scale nodal solutions $u^C_{\beta s}(t')$ inside the coarse time-step

$$u^C_{\beta s}(t') = A(t')\tilde{u}^C_{\beta s} + B(t')\bar{u}^C_{\beta s}, \tag{5.15}$$

where, $\tilde{u}^C_{\beta s}$ and $\bar{u}^C_{\beta s}$ denote the nodal coefficients in the GPCE of the coarse solution at the start and end of the coarse time step (see Fig. 11). $A(t')$ and $B(t')$ are special positive functions that obey the following relations:

$$A(t') + B(t') = 1,\ A(0) = 1,\ A(\Delta t) = 0,\ B(0) = 0,\ \text{and}\ B(\Delta t) = 1. \tag{5.16}$$

Eq. (5.15) involves representation of a function as a convex combination of two functions.

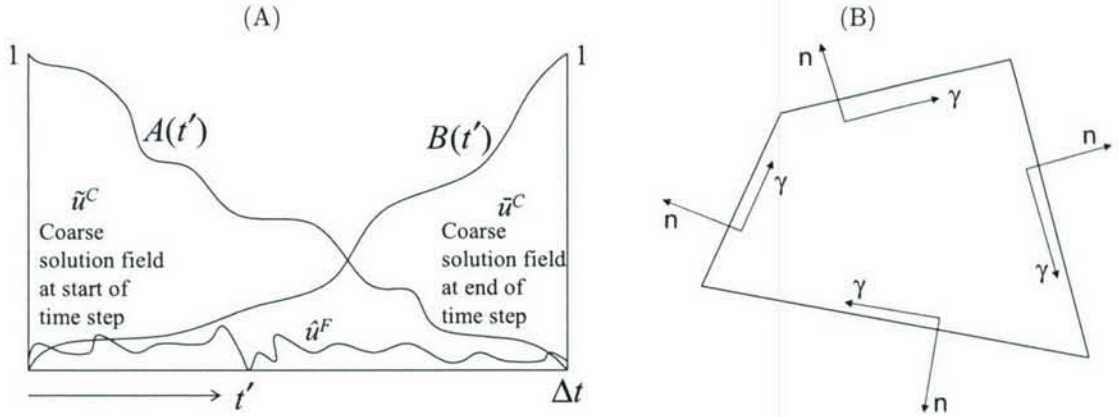

Figure 11: A. Schematic of the time integration framework: Δt is the coarse-time step and t' is the local time coordinate. The integration parameters $A(t')$ and $B(t')$ are shown in the figure. Also, $\tilde{u}^C_{\beta s}$ and $\bar{u}^C_{\beta s}$ are identified as the coarse solution fields at the start and end of the coarse time step, respectively. B. Schematic of a typical coarse element sub-domain: The coordinates normal and tangential to the element edges are denoted by the letters n and γ, respectively.

The representation given in Eq. (5.15) is quite general and incorporates several well-known time integration rules. For example, $A(t') = (\Delta t - t')/\Delta t$ and $B(t') = t'/\Delta t$ yields a backward-Euler time integration rule.

From Eqs. (5.13) and (5.15), we can write the C2S map as follows:

$$\hat{u}^F_{\beta s}(\mathbf{x}, t, \omega) = \sum_{\beta=1}^{Nbf}\sum_{s=0}^{P_C}\left[\tilde{u}^C_{\beta s}A(t')\phi^F_{\beta s}(\mathbf{x}, t', \omega) + \bar{u}^C_{\beta s}B(t')\phi^F_{\beta s}(\mathbf{x}, t', \omega)\right]. \tag{5.17}$$

We can now write Eq. (5.14) as

$$\begin{aligned}
&\tilde{u}^C_{\beta s}\left\{\left(\left\{A(t')(\zeta_s\Psi_\beta + \phi^F_{\beta s})\right\}_{,t}, v^F\right) + \left(k\nabla\left\{A(t')(\zeta_s\Psi_\beta + \phi^F_{\beta s})\right\}, \nabla v^F\right)\right\} + \\
&\bar{u}^C_{\beta s}\left\{\left(\left\{B(t')(\zeta_s\Psi_\beta + \phi^F_{\beta s})\right\}_{,t}, v^F\right) + \left(k\nabla\left\{B(t')(\zeta_s\Psi_\beta + \phi^F_{\beta s})\right\}, \nabla v^F\right)\right\} = 0.
\end{aligned} \tag{5.18}$$

Note that the above equation is fully characterized based on the values taken by $\tilde{u}^C_{\beta s}$ and $\bar{u}^C_{\beta s}$ and the subgrid basis function $\phi^F_{\beta s}$.

We are looking to construct a localized scheme for representation of the subgrid solutions. Further, this localized scheme should hold for all possible values of the coarse nodal coefficients $\tilde{u}^C_{\beta s}$ and $\bar{u}^C_{\beta s}$. Hence, we equate the terms in parentheses to zero to obtain the set of variational formulations defined for each

combination of indices β and s, where, $\beta = 1, \ldots, \text{Nbf}$ and $s = 0, \ldots, \text{P}_\text{C}$. Now, by using the relations $A(t') + B(t') = 1$, we obtain the evolution equation for $\phi^F_{\beta s}$

$$\left((\zeta_s \Psi_\beta + \phi^F_{\beta s})_{,t}\, , v^F \right) + \left(k \nabla (\zeta_s \Psi_\beta + \phi^F_{\beta s}), \nabla v^F \right) = 0. \tag{5.19}$$

Affine correction term The affine correction term u^{F0} as defined by Eq. (5.9) leads to the following strong form of equations inside each coarse element sub-domain

$$u^{F0}{}_{,t} + \nabla \cdot (k \nabla u^{F0}) = f, \ \mathbf{x} \in \mathcal{D}^{(e)}. \tag{5.20}$$

Boundary conditions In order to localize the computation of $\hat{u}$ to a coarse element, we need an approximate specification of its boundary conditions along coarse-element edges. A schematic showing the calculation of boundary subgrid basis functions for the case of a quadrilateral coarse element is shown in Fig. 11. In the VMS simulation, the subgrid basis functions are generated upto a cut-off time (referred here as the *burn-in time*) that is chosen such that the effects of the subgrid component of the initial condition do not affect the coarse solution. This also ensures that the subgrid basis functions capture sufficient information about the heterogeneities at the subgrid scale. Note that the affine correction term does not have any coarse-scale solution dependence, hence, the assumption that this term goes to zero on coarse element boundaries is justified i.e. $u^{F0} = 0$ on coarse element boundaries. Furthermore, we assume that the affine correction is zero at the start of each coarse time-step i.e. $u^{F0}(\mathbf{x}, 0, \omega) = 0$ (note that the initial conditions here refer to the local time coordinate t'=0).

Post-processing: Fine-scale solution reconstruction Let us assume that the coarse-scale solution, the subgrid basis functions and the affine-correction at a particular time-step are $u^C(\mathbf{x}, \omega)$, $\Phi_{\beta 0}(\mathbf{x}, \omega)$ and $u^{F0}(\mathbf{x}, \omega)$, respectively. The time dependence is not shown here for clarity sake. Also, we emphasize that all calculations in this section are performed on the subgrid mesh associated with each coarse element $\mathcal{D}^{(e)}$.

Inside a given coarse element $\mathcal{D}^{(e)}$, we calculate the reconstructed fine-scale VMS solution as follows:

$$u = \sum_{\beta=1}^{\text{Nbf}} \sum_{s=0}^{P_C} u^C_{\beta s} \Phi_{\beta s} + u^{F0}(\mathbf{x}, \omega), \tag{5.21}$$

where, $\Phi_{\beta s} = \phi^F_{\beta s} + \Psi_\beta \zeta_s$, is the sum of coarse and subgrid basis functions defined on $\mathcal{D}^{(e)}$. Let us now consider the GPCE expansions for $\Phi_{\beta s}$ and u^{F0} as follows:

$$\Phi_{\beta s} = \Phi_{\beta 0} \zeta_s = \sum_{r=0}^{P_F} \Phi_{\beta 0 r} \zeta_s \zeta_r, \ u^{F0} = \sum_{r=0}^{P_F} u^{F0}_r \zeta_r, \tag{5.22}$$

wherein, $P_F + 1$ is the number of terms used in the GPCE expansion of $\Phi_{\beta 0}$ and u^{F0}. Now, we can write Eq. (5.21) as follows:

$$u = \sum_{\beta=1}^{\text{Nbf}} \sum_{s=0}^{P_C} \sum_{r=0}^{P_F} u^C_{\beta s} \Phi_{\beta 0 r}(\mathbf{x}) \zeta_r(\omega) \zeta_s(\omega) + \sum_{r=0}^{P_F} u^{F0}_r(\mathbf{x}) \zeta_r(\omega), \ \mathbf{x} \in \mathcal{D}^{(e)}. \tag{5.23}$$

The m-th term in the GPCE of the reconstructed fine-scale VMS solution u can now be written as follows:

$$u_m = \sum_{\beta=1}^{\text{Nbf}} \sum_{s=0}^{P_C} \sum_{r=0}^{P_F} u^C_{\beta s} \Phi_{\beta 0 r} \frac{\langle \zeta_r(\omega) \zeta_s(\omega) \zeta_m(\omega) \rangle}{\langle \zeta_m(\omega) \zeta_m(\omega) \rangle} + u^{F0}_m(\mathbf{x}), \tag{5.24}$$

where, $\langle f(\omega) \rangle$ is used to denote the mathematical expectation of the random function $f(\omega)$.

Numerical Example: Transient diffusion in a two-phase microstructure As an example, a stochastic variational multi-scale formulation was used for addressing transient diffusion problems in random heterogeneous microstructure (Fig. 12(a)) with the stochastic parameter being the diffusion coefficient

having multiple length scales. A gray scale image of a representative two-phase (α and β) microstructure. The intensities (I) are scaled to [0,1]. Let pure α-phase and pure β-phase be associated with scaled intensities $I = 0$ and $I = 1$, respectively.

Probability model – We assume that the pure α and pure β-phases have the following uniformly distributed thermal conductivities.

$$k_\alpha(\omega) = k_{\alpha 0} + k_{\alpha 1}\xi_1(\omega), \text{ and } k_\beta(\omega) = k_{\beta 0} + k_{\beta 1}\xi_2(\omega), \tag{5.25}$$

where, $\xi_1(\omega)$ and $\xi_2(\omega)$ are two independent uniform random variables defined on the interval [-1,1]. We use the following mixture model for defining the thermal conductivity at a given location on the microstructure:

$$k(\mathbf{x}, \omega) = (k_\beta(\omega) - k_\alpha(\omega))I(\mathbf{x}) + k_\alpha(\omega), \tag{5.26}$$

where, $I(\mathbf{x})$ is the scaled intensity at a point $\mathbf{x}$ on the microstructure.

GPCE model – Since the input distribution is uniform (two- dimensional), a two-dimensional, third-order Legendre chaos expansion (yielding a 10 term expansion) was used for representing the solution. The first few terms in the expansion are shown below:

$$\begin{aligned} u(\mathbf{x}, t, \theta) = u_0 + u_1\xi_1(\omega) + u_2\xi_2(\omega) + u_3(3\xi_1^2(\omega) - 1)/2, \\ +u_4\xi_1(\omega)\xi_2(\omega) + u_5(3\xi_2^2(\omega) - 1)/2 + \ldots, \end{aligned} \tag{5.27}$$

The main idea here was to calculate the diffusion dynamics on a highly coarse-mesh by including localized solutions to sub-grid problems. The method captures the mean field (Fig. 12(b)) as well as statistical quantities such as the first order fluctuations (Fig. 12(c)) in the temperature field in a single simulation.

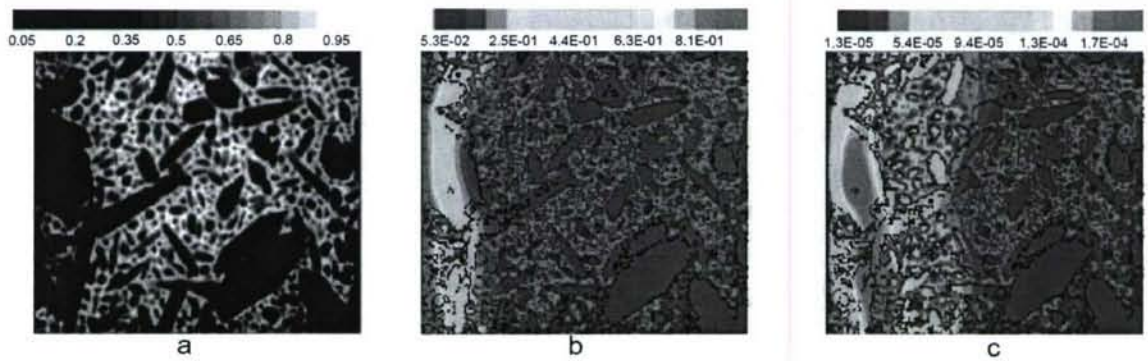

Figure 12: Modeling diffusion in heterogeneous random microstructures using a variational multi-scale algorithm: (a) Microstructure image realization, (b) Mean temperature field (coefficients u0 of GPCE), (c) First-order statistics (coefficient u1 in the GPCE).

6 Development of maximum entropy techniques for modeling topological uncertainties in polycrystalline metallic microstructures

Probability distribution functions (PDFs) providing a complete representation of microstructural variability in 3D polycrystalline materials using limited information is difficult to obtain since this inverse problem is highly ill-posed. We use the maximum entropy (*MaxEnt*) principle to compute a PDF of microstructures based on given information about a microstructural system. Microstructural features are incorporated into the maximum entropy framework using data obtained from experiments or simulations. Statistics of material properties are then extracted by interrogating sample microstructures obtained from the resultant probability distribution function (PDF). These property statistics are important because they give a numerical estimate

of how the material may perform when subjected to extremal conditions. A particular problem of interest addressed here is the determination of effective behavior of three-dimensional (3D) polycrystalline materials based on uncertainties induced due to randomness in grain distribution and texture of microstructures.

Some important concerns which are addressed in this work are: (i) how to quantify uncertainties in the micro-scale based on limited observable behavior at the macroscale, (ii) how to model polycrystal microstructures and obtain microstructural samples incorporating the uncertainties computed above, and (iii) how to obtain statistics of homogenized plastic properties from this statistical description of microstructures. In obtaining the distribution from which microstructures are sampled, we use the principle of maximum entropy (*MaxEnt*). *MaxEnt* is a popular technique that is utilized to construct the PDF for stochastic fields when limited information is available about them. Availability of limited information is often the case due to high-costs involved in performing a large number of experiments or simulations. For instance, grain size distributions of polycrystalline materials cannot be experimentally measured easily since they vary even at a material point for different samples of the material. Such serious limitations on the measurability of stochastic fields has made *MaxEnt* an immensely popular choice amongst statisticians. To make this method feasible, information-theorists developed a mathematical tool for measuring entropy of systems. Given a random variable x which takes discrete values given by $x_1, x_2, \ldots, x_n$, the informational entropy of x is given by

$$\mathbf{H}(p) = -\sum_{i=1}^{n} p(x_i) log(p(x_i)) \tag{6.1}$$

where $p(x_i)$ denotes probability of the discrete event x_i occurring. Suppose we have insufficient knowledge about the distribution p. *MaxEnt* provides a rationale to obtain the entire probabilistic variability about the variable x. It is to be noted that the entropy function $\mathbf{H}(p)$ is convex and in an unconstrained problem, it achieves its maximum value when all the possible events x_i are equiprobable. This occurs when all of the $p(x_i)$ are equal. We call this particular choice of $p(x_i)$ as $q(x_i)$. The distribution $q(x_i)$ does not lead to maximum entropy when there is some knowledge about the system x, which denotes the vector of variables x_i. To distinguish a random variable from a random field, we use the notation $\mathbf{x}$ for the latter. Typical knowledge about microstructural systems of polycrystalline materials is given in the form of lower-order statistical moments of grain sizes as well as average texture values in the form of an orientation distribution functions (ODF). These known moments are denoted as M_i. Features such as grain sizes and ODFs are denoted as f_i. Knowledge about microstructural features, which can be computed using experiments or simulations, is posed as a constraint for the *MaxEnt* optimization problem which is mathematically stated as follows:

$$Find : p^*(\mathbf{x}) = \arg\max_{p} \mathbf{H}(p)$$

with the given constraints

$$\begin{aligned} M_1 &= \mathbf{E}(f_1(\mathbf{x})) \\ M_2 &= \mathbf{E}(f_2(\mathbf{x})) \\ &\vdots \\ M_N &= \mathbf{E}(f_N(\mathbf{x})) \end{aligned} \tag{6.2}$$

where $\mathbf{E}$ denotes expectations over the space of random variables. When considering topological uncertainties within a microstructure (Problem 1 in Section 5), we define the operator $\mathbf{E}$ for grain size feature over the set of grains within a microstructure as given below:

$$\mathbf{E}(f(\mathbf{x})) = \frac{1}{G}\sum_{i=1}^{G} f(x_i) \tag{6.3}$$

where G is the number of grains in the microstructure and f represents the grain size feature. The t^{th} moment of a specific feature f_i is computed as $\mathbf{E}(f_i^t)$. The distribution that is finally computed, $p^*(\mathbf{x})$

is the most uniform distribution satisfying the given constraints in Eq. (6.2). This means that $p^*(\mathbf{x})$ is closest in distance to $q(\mathbf{x})$ while satisfying the available information about the system given by Eq. (6.2). A popular choice of distance measure is the Kullback-Leibler (KL) divergence measure. For any two arbitrary probability distributions, m and n, the KL divergence is given as follows:

$$KL(m||n) = \sum_i m(x_i) log \frac{m(x_i)}{n(x_i)} \tag{6.4}$$

Hence, the distribution $p^*(\mathbf{x})$ satisfies the additional property that:

$$p^*(\mathbf{x}) = \arg\min_p KL(p||q) \tag{6.5}$$

while satisfying Eq. (6.2). This KL divergence measure is crucial in reconstructing microstructures based on grain size distributions. The problem of computing a probability distribution $p(\mathbf{x})$ given the constraints in Eq. (6.2) is ill-posed. *MaxEnt* is a technique that is able to establish a unique PDF $p^*(\mathbf{x})$ that satisfies the given information. The maximum entropy technique makes the problem well-posed by imposing additional restrictions on the computed PDF. Utilizing the microstructural features such as grain sizes and ODFs (f_i), the PDF that is obtained using the *MaxEnt* technique is of the following form:

$$p^*(\mathbf{x}) = \frac{e^{-\sum_{n=1}^{N} \lambda_n f_n(\mathbf{x})}}{\int e^{-\sum_{n=1}^{N} \lambda_n f_n(\mathbf{x})} d\mathbf{x}} \tag{6.6}$$

where λ_i represent the Lagrange multipliers that account for the N system constraints. This exponential form as seen in Eq. (6.6) is a very central concept in the *MaxEnt* formalism. A number of numerical options are available to compute a microstructural system that has maximum entropy within its features while simultaneously satisfying given information about the system. A Gibbs sampler is used that starts from a random microstructure and after a period known as burn-in, generates microstructures that are sampled from PDFs of the form given in Eq. (6.6). Samples generated after the burn-in period are accepted as microstructural samples from the desired distribution. The algorithm for grain sizes follows closely the algorithm given in [10, 11].

Numerical Example: Variability in Aluminum polycrystals driven by mean grain sizes: Literature is replete with many instances of phenomenon such as Hall-Petch effect that depend only on the mean grain size. In such a situation, the variability of grain sizes within a microstructure becomes superficial since clearly, different distributions may represent the same mean grain size. Hence, we extract a different feature which quantifies how mean grain sizes vary across different samples. The *MaxEnt* distribution is defined over a set of microstructures, each characterized by its mean PDF. Potential applications of this example relates to predicting statistical behavior of random polycrystals where the behavior is a function of mean grain sizes.

This problem is driven by variability in mean grain sizes of different given Aluminum microstructural samples. The variability in mean grain sizes as well as textures are utilized to define a PDF of microstructures. Based on samples from this PDF and using a homogenization scheme [6], we compute bounds in the plastic stress strain curve of Aluminum. Using input microstructures generated (Fig. 13) from 3D-phase field simulations, we compute the expected grain sizes (volumes) of each microstructure.

Lower moments until the fourth-order of these (mean) grain sizes are extracted and a maximum entropic distribution is computed. We use just five input microstructures because in practice, it may prove costly to compute experimental microstructures at different material points. Hence, the input information relies only on the limited set of microstructural samples. The resultant distribution based on two, three and four mean-grain size moments is depicted in Fig. 14. Each point in the $x - axis$ corresponds to a microstructure with the corresponding value as the mean grain size. Hence, the PDF just represents the probabilities of the corresponding microstructures.

The *MaxEnt* distribution was computed using the stabilized version of the conjugate gradient algorithm. The computed distribution also shows that the randomness induced due to *MaxEnt* reduces as we incorporate more information about the source of randomness (incorporated using higher moments). We compute voronoi-cell microstructures which are sampled from the *MaxEnt* distribution.

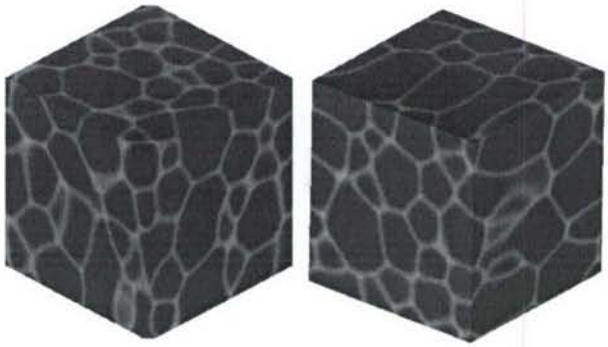

Figure 13: Two out of the five samples of microstructures computed using phase field technique that was used in problem 1.

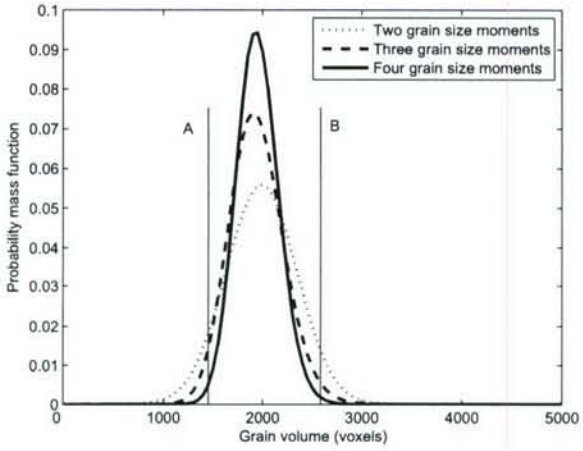

Figure 14: A *MaxEnt* distribution of mean grain sizes based on inputs from 3D phase-field simulations.

Further, samples from the tail of the *MaxEnt* distribution were computed to obtain bounds on the plastic properties. Samples near the tails are computed as follows: Start randomly sampling from the *MaxEnt* distribution till a sample which falls outside the 95% confidence region is reached. 95% confidence region is the region where 95% of random samples are expected to lie and this is distributed evenly on either side of the mean. This is accepted as a tail sample. We choose one tail sample from each extreme of the *MaxEnt* distribution. Each sample computed from the PDF corresponds to a microstructure with the corresponding mean grain size. Some microstructures that were sampled from the tail are shown in Fig. 15. These were meshed using the commercially available software CUBIT using hexahedral meshes.

Finally, a rate-independent homogenization method is utilized to compute bounds of the non-linear plastic properties of the reconstructed microstructures based on a simple tension test using a strain rate of 0.01 per second. Bounds in the properties based on a set of 25 samples are shown in Fig. 16.

The variability results due to difference between mean grain sizes of these microstructures. Tails of this distribution correspond to extremes of mean grain size and were crucial in defining bounds on the material behavior of Aluminum polycrystals. We also saw how the incorporation of different amounts of information resulted in stricter bounds. Mathematical characterization of such distributions between microstructures pose potential applications in stochastic simulations such as SSFEM which are still driven by analytical assumptions. Further, statistical characterizations of phenomenon such as Hall-Petch effect can be made using the variability in mean grain sizes.

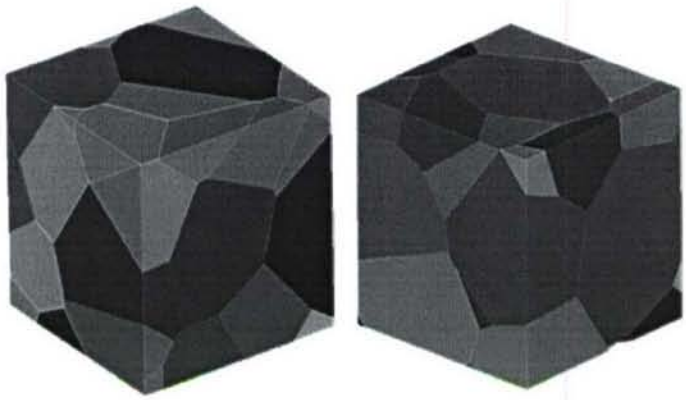

Figure 15: Samples obtained at locations A and B of Fig. 14.

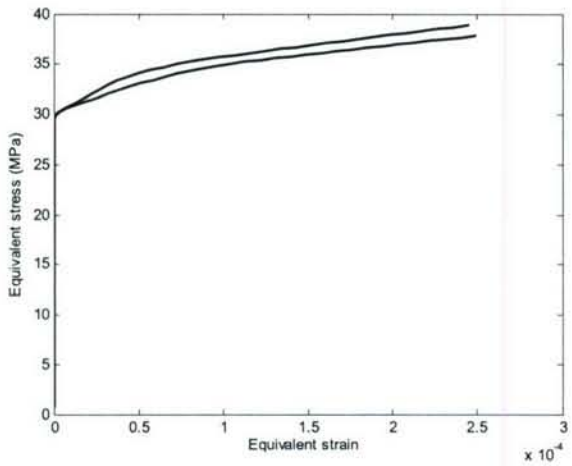

Figure 16: Bounds of the material strength computed from microstructures sampled near the tail of *MaxEnt* distribution.

Acknowledgment/Disclaimer

This work was sponsored (in part) by the Air Force Office of Scientific Research, USAF, under grant/contract number FA9550-04-1- 0070. The views and conclusions contained herein are those of the authors and should not be interpreted as necessarily representing the official policies or endorsements, either expressed or implied, of the Air Force Office of Scientific Research or the U.S. Government.

Personnel supported during duration of grant

N. Zabaras (PI), B. Velamur asokan (GRA), S. Acharjee (GRA - supported in part), V. Sundararaghavan (GRA - supported in part), S. Sankaran (GRA - supported in part).

References

[1] S. Acharjee and N. Zabaras, "Uncertainty propagation in finite deformations – A spectral stochastic Lagrangian approach", Computer Methods in Applied Mechanics and Engineering, Vol. 195, pp. 2289-2312, 2006

[2] S. Acharjee and N. Zabaras, "A non-intrusive stochastic Galerkin approach for modeling uncertainty propagation in deformation processes", Computers and Structures (special issue on Stochastic Modeling, G.I.Schueller, edt.), Vol. 85, Issues 5-6, pp. 244-254, 2007

[3] S. Acharjee and N. Zabaras, "A concurrent model reduction approach on spatial and random domains for stochastic PDEs", International Journal for Numerical Methods in Engineering, Vol. 66, pp. 1934-1954, 2006.

[4] S. Ganapathysubramanian and N. Zabaras, "Design across length scales: A reduced-order model of polycrystal plasticity for the control of microstructure-sensitive material properties", Computer Methods in Applied Mechanics and Engineering, Vol. 193 (45-47), pp. 5017-5034, 2004.

[5] S. Ganapathysubramanian and N. Zabaras, "Modeling the thermoelastic-viscoplastic response of polycrystals using a continuum representation over the orientation space", International Journal of Plasticity, Vol. 21/1 pp. 119-144, 2005

[6] V. Sundararaghavan and N. Zabaras, "Design of microstructure-sensitive properties in elasto-viscoplastic polycrystals using multi-scale homogenization", International Journal of Plasticity, Vol. 22, pp. 1799-1824, 2006

[7] S. Acharjee and N. Zabaras, "The continuum sensitivity method for the computational design of three-dimensional deformation processes", Computer Methods in Applied Mechanics and Engineering, Vol. 195, pp. 6822-6842, 2006

[8] B. Velamur Asokan and N. Zabaras, "Variational multiscale stabilized FEM formulations for transport equations: stochastic advection-diffusion and incompressible stochastic Navier-Stokes equations", Journal of Computational Physics, Vol. 202/1, pp. 94-133, 2005

[9] B. Velamur Asokan and N. Zabaras, "A stochastic variational multiscale method for diffusion in heterogeneous random media", Journal of Computational Physics, Vol. 218, pp. 654-676, 2006

[10] S. Sankaran and N. Zabaras, "A maximum entropy approach for property prediction of random microstructures", Acta Materialia, Vol. 54, pp. 2265-2276, 2006.

[11] S. Sankaran and N. Zabaras, "Computing property variability of polycrystals induced by grain size and orientation uncertainties", Acta Materialia, Vol. 55, Issue 7, pp. 2279-2290, 2007.

[12] N. Zabaras and S. Sankaran, "An information-theoretic approach to stochastic materials modeling", IEEE Computing in Science and Engineering (CiSE), special issue of "Stochastic Modeling of Complex Systems",March/April issue, pp. 50-59, 2007.

[13] B. Velamur Asokan and N. Zabaras, "Using stochastic analysis to capture unstable equilibrium in natural convection", Journal of Computational Physics, Vol. 208/1, pp. 134-153, 2005.

[14] V. Sundararaghavan and N. Zabaras, "On the synergy between classification of textures and deformation process sequence selection", Acta Materialia, Vol. 53/4, pp. 1015-1027, 2005.

[15] Velamur Asokan Badri Narayanan and N. Zabaras, "Stochastic inverse heat conduction using a spectral approach", International Journal for Numerical Methods in Engineering, Vol. 60/9, pp. 1569-1593, 2004

[16] L.L. Graham-Brady, S.R. Arwade, D.J. Corr, M.A. Gutierrez, D. Breysse, M. Grigoriu, N. Zabaras, "Probability and materials, from nano- to macro-scale: A summary", Probabilistic Engineering Mechanics, Vol. 21, pp. 193-199, 2006.

PhD Thesis

- Badrinarayanan Velamur Asokan, "Variational multiscale method for stochastic thermal and fluid flow problems", Ph.D. Dissertation (defended on April 25, 2006), Sibley School of Mechanical and Aerospace Engineering, Cornell University, May 2006 (Currently at Oak Ridge National Laboratory (ORNL), TN).

- Swagato Acharjee, "Stochastic and deterministic techniques for computational design of deformation processes", Ph.D. Dissertation (defended on April 13, 2006), Sibley School of Mechanical and Aerospace Engineering, Cornell University, May 2006 (Currently at Merrill Lynch, UK).

- Veera Sundararaghavan, "Multi-scale Computational Techniques for Design of Polycrystalline Materials", Ph.D. Dissertation (defended on May 18, 2007), Sibley School of Mechanical and Aerospace Engineering, Cornell University, August 2007 (Joining faculty of Aerospace engineering at University of Michigan, Ann Arbor).

Conference presentation slides and preprints of the above papers are available for download at our web-site http://mpdc.mae.cornell.edu

Honors and Awards

Received ASME Fellow-awarded 2006

Transitions

- The PI has reviewed this project in various agencies such as AFOSR, NSF, AFRL and NIST and in several conferences such as USNCCM, NUMIFORM, TMS and WCCM.

- The Army's Small Business Technology Transfer (STTR) Program solicitation A06-T009 Performance Map for Low-Cost Titanium Armor in 2006 has listed our work as a key reference.

- The National Science Foundation funded a workshop entitled Probability and Materials: from Nano- to Macro-Scale at Johns Hopkins University on January 57, 2005. The goal of this workshop was to bring together a diverse multi-disciplinary and multi-skilled group of researchers, all of whom have an interest in the application of probabilistic models to multi-scale analysis of materials. A set of recommendations for important future research in probability and materials was proposed by the group and is provided in the reference [16].

New Discoveries

(a) The first stochastic variational multi-scale algorithm with explicit subgrid modeling reported; (b) The first techniques reported for full-probabilistic modeling and design of deformation processes (c) Multi-scale computational simulator for design of mechanical properties such as stiffness and strength during deformation processes by tailoring underlying microstructures (d) New techniques for reconstruction of 3D microstructures from limited statistical information (e) Techniques for computing property variabilities due to topological uncertainties in the microstructure.